Dynamic Modeling, Simulation, and Testing of a Marine DC Hybrid Power System

Pramod Ghimire, *Student Member, IEEE*, Mehdi Zadeh, *Member, IEEE*, Eilif Pedersen, *Member, IEEE*, Jarle Thorstensen

***Abstract*—The hybridization of power systems offers the low-emission and energy-efficient marine vessels. However, it increases the complexity of the power system. Design, analysis, control, and optimization of such a sophisticated system require reliable and efficient modeling tools to cover a wide range of applications. In this work, a typical DC hybrid power system model is developed using a bond graph modeling approach. Necessary component models of varying degrees of fidelity are developed and integrated to build a system model with reasonable accuracy. The developed system model, along with the rule-based energy management system, is used to simulate the entire system and to investigate the load-sharing strategies as well as the system stability in various operating scenarios. Moreover, the simulation results are validated with experimental results conducted on a full-scale laboratory setup of DC hybrid power system and with a ship load profile. The results show that the system model is capable of capturing the fundamental dynamics of the real system. The hybrid power system model is further used to analyze the bus voltage deviation from its nominal value. The computational efficiency presented by the system is fairly good as it can simulate faster than real-time. The developed system model can be used to build up a comprehensive simulation platform for different system analysis and control designs.**

***Index Terms*—Marine hybrid power systems, onboard DC power systems, modeling, stability, power and energy management**

I. Introduction

THE International Maritime Organization (IMO) has proposed stringent regulations to reduce emissions and improve energy-efficiency from the shipping industry. The energy-efficiency, low-, zero-emission, and innovative technologies are being investigated to comply with the regulations [1]. The energy storage device (ESD) based zero-emission vessel is still challenging for all types of marine vessels due to the low energy density of ESDs [2], [3]. The low energy density of ESD is compensated by the conventional engine in the marine hybrid power system. The better energy-efficiency, flexibility, and reliability are achieved using hybrid power system [4]. Moreover, it helps in reducing emission and average fuel consumption by optimizing the conventional engine operation for various operating modes [5]. Besides, life cycle assessment shows that it is more environment-friendly compared to conventional power systems [6].

Fuel consumption and emission reduction can be up to 10-35 % through hybrid architecture and advanced control systems [7]. The fuel consumption in a hybrid power system reduces through different operating modes such as peak shaving, load leveling, zero-emission operation, spinning reserve, and strategic loading [8]. The strategic loading of the generator and ESD was modeled and experimentally validated in [9]. Besides, the model was able to estimate fuel oil consumption and NO_x emission. The presence of ESDs in the power system enhances the utilization of shaft generators actively in waves [10], reducing the speed fluctuation for a cargo vessel with an AC power system.

AC power system has been prevailing because of the well-developed control, safety, and voltage transformation systems. However, it possesses the complexities when it comes to harmonics, synchronization, and fixed speed operation. On the contrary, the DC power system eases the complexities of the AC system but lags the well-developed control and safety system for higher voltage levels. With the improvement in safety and advanced control systems, the implementation of the emerging DC power system in a marine vessel is increasing. The additional degrees of freedom are being opened for engine and generator with the utilization of DC distribution systems in hybrid power generation [11]. The frequency independence in the DC power system allows the conventional engines to run at the optimal speed according to the load demand while minimizing the fuel consumption and emission. Moreover, the onboard DC power system allows easy interconnection of ESDs into the grid. The system-level analysis of low-voltage DC hybrid power systems through simulation results was performed in [12], where the physical component models and their integration as a system are discussed, focusing on the power converters. However, the control strategies required for the operation of the complete system are not discussed, and the simulation results are not tested with the experimental results. The discrete-time approach has also been applied to the modeling of onboard DC power systems to deal with the nonlinear dynamics of the power electronics such as the switching related dynamics and the nonlinear behavior of the loads [13]. This model has been tested on a small-scale DC

Manuscript received June 08, 2020; revised August 08, 2020; accepted September 01, 2020. *(Corresponding author: Mehdi Zadeh)*

The authors would like to thank the Research Council of Norway and Kongsberg Digital AS, Norway for financially supporting this work.

Pramod Ghimire (pramod.ghimire@ntnu.no) is with Department of Marine Technology, Norwegian University of Science and Technology (NTNU) and Kongsberg Digital (KDI), Norway.

Mehdi Zadeh (mehdi.zadeh@ntnu.no) is with Department of Marine Technology, NTNU, Norway.

Eilif Pedersen (eilif.pedersen@ntnu.no) is with Department of Marine Technology, NTNU, Norway.

Jarle Thorstensen (jarle.thorstensen@kdi.kongsberg.com) is with KDI, Norway.

power system and seems to be challenging to extend to large scale systems.

As the DC power system is a complex system with high dynamics, it requires a new and intricate power system design along with advanced control and load-sharing algorithms for optimal and reliable operations [14]. In a hybrid power system, power and energy management must handle the load scheduling and sharing algorithms between ESDs and conventional engines. Moreover, it regulates and stabilizes the power system under load changes. An energy management strategy for a hybrid DC microgrid, consisting of a generator and supercapacitor, was presented in [15] along with laboratory validation.

The design and analysis of different aspects, such as stability analysis, failure mode identification, and mitigation, and advanced control architectures, of such a complex system, require a useful tool including system modeling and simulation. One of the advantages of a complete system model is its application as an integrated simulator platform that can be used to simulate and analyze 'what-if' scenarios in the hybrid power system. These scenarios can be normal operating or failure conditions. Besides, due to the increase in computational power, the use of big data is increasing for different data-based tools like machine learning and artificial intelligence [16]. A reliable and tested power system simulator can be a source of data generation for training their algorithms.

To achieve efficient system modeling, modularity in the component models is essential. The library of component models for an AC marine power system, without the hybrid power system components, was developed to enhance modularity [17], where the models were tested against the full-scale measurement from a supply vessel. Modularity also enhances the reconfiguration of a system model. The reconfiguration possibility in a marine vessel and power plant simulator was presented in [18]; however, it lacks quantitative verification. The real-time simulation is necessary to interface the simulator with the real hardware, hardware-in-the-loop (HIL) or the control systems [19]. A real-time simulator framework for the AC marine power plants with the weak power grid was presented in [20], which also contributed to the study of the numerical stability of hybrid causality generator models. Besides time-domain simulation, the power system models are used to analyze the stability of the system [21], [22], and also to evaluate the performance of the system with the nonlinear dynamics [23]. Moreover, simulation of faults and abnormal conditions at the component and the system levels enhance the testing and training of the complex power system.

In recent years, dynamic models have been established and used in the simulation tools for complex marine power systems. The required computational effort has always been a challenge in simulating those systems. The computational effort in power system simulation is due to the single matrix formulation, system order, complex switching models, integration step size, and so on [24]. Different techniques have been tested to deal with the computational complexity, such as the proper utilization of computer hardware and more efficient computation. In [25], a parallel processing technique was proposed for power system simulation in a multi-core computer such that the complex system model can be divided into subsystems and solved separately in different cores. In [21], reduced-order models for the power converters in the DC power system are used for efficient simulation and stability analysis. Similarly, efficient power system simulation is achieved by the integration of various fidelity components models in [26]. The parallel processing of the system substantially increases the computational speed. Besides, the accuracy of the results is maintained through the use of high fidelity models. However, care needs to be taken while dividing a system into subsystems to run them in the different cores. The division of a tightly coupled system into subsystems may result in the numerical instability issues [27]. On the contrary, the model order reduction may reduce the accuracy of the system model while maintaining the computational speed and stability. Thus, based on the objective of the simulation, the proper method has to be selected so that the simulation results with acceptable accuracy can be achieved at a reasonable speed. The marine power system simulators are being developed both in academic and industrial sectors for research, training, or engineering objectives. Various institutions and their power system simulators are listed in [18], namely, Marine Cybernetic's Cybersea, U.S. Office of Naval Research's Electric Ship Research and Development Consortium, NTNU's Marine System Simulator (MSS), Kongsberg Digital's K-Sim® simulators, and so on. These simulators use different system models based on the application and usually are designed for low computational effort. However, there is still a need for the dynamic models that could capture the power system dynamics and can be used for the stability analysis and design of both low- and high-level control systems.

A system model can be developed by integrating various components and control system models. The higher the number of component models, the higher will be the complexity and computational effort. The modularity within the system allows the fidelity-selection of the component models depending on the purpose of the simulation. A practical model should be able to run in nearly real-time, integrate various fidelity components and control system models, and accept external load profile. There exist various modeling approaches for system modeling and analysis. The bond graph is an energy-based physical system modeling methodology in which the dynamics between the systems or the components in a system are represented by the exchange of energy [28]. The power variables (effort and flow) represent the energy exchange between the ports of the elements using the power bonds. The product of these power variables gives instantaneous power (rate of energy), which is integrated to calculate the energy transferred. This modeling technique can be used to model the systems in multiple energy domains such as mechanical, electrical, hydraulic, chemical, and so on. It is also easier to interlink systems with various energy domains. The graphical representation enhances the system overview and modularity. The causality strokes in the power bonds indicate the inputs and outputs in the components and systems [29]. The indication of algebraic loops and constraints in the model is obtained during the modeling process, which allows the modeler to make necessary modifications well ahead in time. Besides, easier extractions of mathematical equations leverage

its application for the analytical studies. Bond graph-based models can be converted or combined to the block diagram models such that control engineers can use the physical system models even without prior knowledge of the bond graph modeling technique. However, it is complex to model the distributed systems (partial differential equations) [30] and multiple energy interactive systems [31] like thermal fluids in bond graph technique. The distributed systems can be modeled in this technique by approximating a large number of lumps resulting in the large state-space model, whereas thermal fluids are modeled using a pseudo-bond graph technique [28].

The use of a real physical asset for design, testing, and operational training of the system usually increases both the cost and risk. The use of dynamic system models usually fulfills the criteria for those objectives if the system behavior is realistic. Thus, a system model testing is necessary to ensure confidence in the system behavior. In general, model validations are performed on a laboratory scale. However, the system behavior may vary with the power level due to which not all the responses in the full-scale system may be observed in the laboratory scale [32]. A full-scale test facility dedicated to the marine hybrid power system along with the high-level control systems is presented in [1]. Similarly, a flexible testbed capable of operating at MW power level that can be switched between the medium voltage DC and high-frequency AC power system topologies is presented in [32].

Most of the literature presents different methods and fidelity of component models in a marine power system; however, the complete system modeling is not well-represented despite its importance in analyzing the interactions between the components. Also, the DC marine hybrid power system is one of the less explored research areas compared to other conventional power systems. The complete model of such a complex system that offers acceptable accuracy and real-time simulation capability is lacking.

In this paper, a holistic dynamic model of the DC marine hybrid power system is developed, based on the bond graph modeling approach. Both the low- and high-level control systems required to regulate various control objectives in the component and system levels are developed. The modeled simulator is able to capture the power system dynamics with acceptable accuracy while maintaining real-time computation. The contribution of this model is to cover the whole ship power system and to consider the necessary dynamics for each part of the system, meaning that there is no compromise in the system dynamics. The proposed model is also validated with experimental results from a full-scale laboratory setup of the DC hybrid power system [1]. A scaled ship load profile is used as the test power profile. A rule-based energy management system (EMS) is used for load-sharing and control under load changes. The system model simulates various operating strategies and dynamic conditions such as load power variation, load speed variation, and failure conditions. Moreover, the developed system model is used to analyze the bus voltage variation in the real experimental setup. Since the dynamic models are core establishing parts of the large scale simulators, it is essential to have a reliable model that can be modular, scalable and at the same time computationally efficient. The proposed method is not outperforming the large scale simulators; instead, it is presented as an efficient dynamic model that can be used either in time-domain simulation tools or in the analytical studies for system and control design.

This paper is divided into six sections. The system overview, along with component models, is described in section II. Section III discusses the overall control structure in a DC hybrid power system. Section IV includes the results from the system simulation, while section V compares the experimental and simulated results. The conclusion of the work is presented in section VI.

II. Modeling of the DC Hybrid Power System

The simplified schematic of a hybrid power system, modeled in this work, is included in Fig. 1. The main DC bus is sectionalized through a bus-tie breaker that remains closed in regular operation. Two variable speed diesel engines are driving their respective synchronous generators, which are interfaced to the bus through the uncontrolled rectifiers. The bidirectional DC-DC converters are connecting two battery banks to the bus. Two three-phase induction motors, emulating the propulsion loads, are driven by voltage source inverters (VSIs).

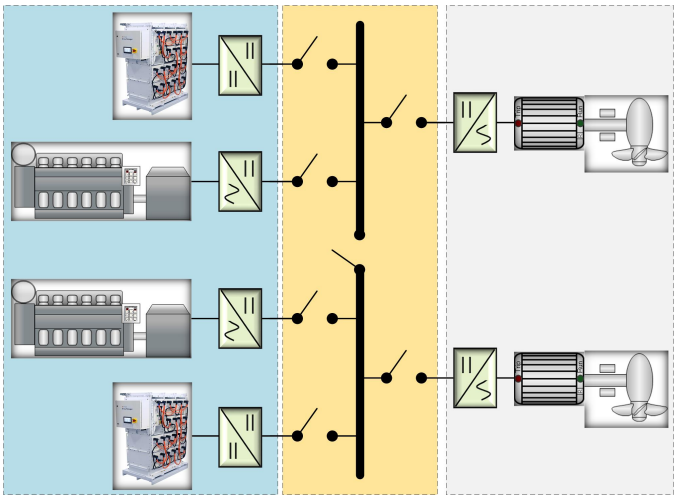

Fig. 1: Schematic of the studied DC hybrid power system.

A. Generator Set

A simplified diesel engine is modeled based on [20] as,

$$\dot{\omega}_m = \frac{1}{J_m + J_G}(T_m - b_f\omega_m - b_b\omega_m^n - T_e) \tag{1}$$

$$\dot{\theta}_m = \omega_m \tag{2}$$

where ω_m and θ_m are the angular speed and position, J_m is engine inertia, J_G is generator inertia, T_m is mechanical torque, T_e is generator's electromagnetic torque, b_f is friction parameter, b_b is the braking parameter, and n is a constant, typically 0.1. T_m, generated by the combustion of the fuel, is given by the ratio of effective engine power P_e and angular speed ω_m.

$$T_m = \frac{P_e}{\omega_m} = \frac{\dot{m}_f h_n \eta}{\omega_m} \tag{3}$$

where, $\dot{m}_f$ is the inlet fuel flow rate and h_n is the lower calorific heat value (LHV) of the fuel. The engine efficiency is expressed as $\eta = (SFC \cdot h_n)^{-1}$, where h_n is in MJ/kg and specific fuel consumption SFC is in mg/J. Moreover, SFC, as a function of P_e, is expressed as $SFC = \dot{m}_f \cdot {P_e}^{-1}$. The two-axis-model of synchronous generator [33], with current as an output variable, is given as,

$$\dot{\boldsymbol{\Psi}} = -\omega_m \boldsymbol{D}\boldsymbol{\Psi} - \boldsymbol{R}\boldsymbol{i} + \boldsymbol{E}\boldsymbol{u_{d,q}} + \boldsymbol{b}u_f \tag{4}$$

$$\boldsymbol{i} = \boldsymbol{L^{-1}}\boldsymbol{\Psi} \tag{5}$$

where, $\boldsymbol{\Psi} = [\Psi_d, \Psi_q, \Psi_f, \Psi_D, \Psi_Q]^T$ is the magnetic flux vector, $\boldsymbol{i} = [i_d, i_q, i_f, i_D, i_Q]^T$ is current vector, $\boldsymbol{u}_{d,q} = [u_d, u_q]^T$ is voltage vector, and u_f is field voltage. Similarly, $\boldsymbol{D}$ is a pole-pair matrix, $\boldsymbol{E}$ is a matrix coefficient for a voltage vector, $\boldsymbol{b}$ is a matrix coefficient for a field voltage, $\boldsymbol{R}$ is the internal resistance matrix, and $\boldsymbol{L}$ is the inductance matrix. In the weak power grids, like shipboard grids, the voltage and frequency of the system may vary with high load power transients. Moreover, any generator must be able to operate in voltage control mode while allowing the other generators to operate in standby or current control mode for optimal operation. The voltage-output model for the synchronous generator is expressed as,

$$\boldsymbol{u_{d,q}} = \dot{\boldsymbol{\Psi}}_{d,q} + \omega_m \boldsymbol{D}_{d,q}\boldsymbol{\Psi}_{d,q} + \boldsymbol{R_{d,q}}\boldsymbol{i_{d,q}} \tag{6}$$

Since direct differentiation poses the risk of instability, the derivatives of magnetic fluxes are calculated using a low pass filter with a derivative effect [20]. The electromagnetic torque generated is expressed as,

$$T_e = n_p(\psi_d i_q - \psi_q i_d) \tag{7}$$

where, n_p is the number of pole pairs. A hybrid causality synchronous generator model, which can switch between the voltage- and current-output on the fly [17], [20], is implemented along with an added parameter calculation block.

B. Propulsion Unit

The propulsion units are modeled as induction motor based on the two-reaction-theory [17], [33]. The mathematical equations for an induction motor can be expressed as,

$$\boldsymbol{u_m} = \boldsymbol{R_m}\boldsymbol{i_m} + \frac{d\boldsymbol{\psi_m}}{dt} + \omega_m \boldsymbol{D_m}\boldsymbol{\psi_m} \tag{8}$$

$$\boldsymbol{i_m} = \boldsymbol{L_m}^{-1}\boldsymbol{\psi_m} \tag{9}$$

$$T_{em} = n_p(\psi_{ds} i_{qs} - \psi_{qs} i_{ds}) \tag{10}$$

$$\omega_m = \frac{1}{J_m}\int (T_{em} - T_{Lm} - T_{fm})dt \tag{11}$$

where T_{em}, T_{Lm}, and T_{fm} are electromagnetic, load, and frictional torque, respectively and J_m is motor inertia. The voltage, current and flux linkage vectors are respectively represented as $\boldsymbol{u_m}$, $\boldsymbol{i_m}$, and $\boldsymbol{\psi_m}$. Similarly, $\boldsymbol{R_m}$, $\boldsymbol{L_m}$, and $\boldsymbol{D_m}$ are resistance, inductance, and pole-pair matrices, respectively. The load torque exerted by the propeller is an input to the induction motor, which can be defined in the load model or can be read from the look-up table.

C. Lithium-ion Battery

In this work, lithium-ion battery packs are used as the energy storage devices (ESDs). A Thevenin-based first-order electrical circuit model for lithium-ion battery pack is implemented based on the model presented in [34], [35]. The electrical circuit model and its analogous bond graph-based model is shown in Fig. 2. The effect of temperature, number of cycles, and self-discharging are not considered in this case. The open-circuit voltage V_{oc} of a battery depends on the electrolyte temperature T in Kelvin and state of charge SoC as,

$$V_{oc} = V_{oc0} - K_e T(1 - SoC) \tag{12}$$

where, V_{oc0} is initial open-circuit voltage, and K_e is battery parameter. The dynamic behaviour of the battery is captured by its impedance. The output resistor (R_0) and the parallel combination of resistor (R_1) and capacitor (C_1) are calculated as in (13) - (15), where R_{00} and R_{10} are initial resistances, a_0 is battery parameter, and τ_1 is battery time constant.

$$R_0 = R_{00}(1 + a_0(1 - SoC)) \tag{13}$$

$$R_1 = -R_{10} ln(1 - SoC) \tag{14}$$

$$C_1 = \frac{\tau_1}{R_1} \tag{15}$$

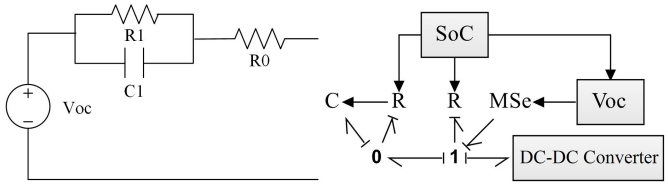

Fig. 2: Lithium-ion battery models, (a) electric circuit model (b) bond graph model.

D. Converters

1) Uncontrolled Rectifier: Since the bus voltage can be regulated using an automatic voltage regulator, the uncontrolled rectifier is modeled to interface synchronous generator to the bus. A three-phase, full-wave, diode rectifier circuit diagram, and different modeling approaches are explained in [36]. Two different rectifier models are required for connecting hybrid synchronous generator model outputs to the bus. An average rectifier is modeled in the dq-reference frame based on [17]. The mathematical equations for the rectifier when the generator is operating in the voltage-output mode are given in (16) - (21), where U_{RMS} is RMS line-to-line voltage, I_{RMS} is RMS current, ω is the angular frequency of the generator, Ls is generator side inductance, I_{DC} is the average DC current, η is converter efficiency, and PF is the power factor. P and Q are active and reactive power. i_d, u_d, i_q, and u_q are current

and voltage in d- and q-axes, respectively.

$$U_{RMS} = \sqrt{\frac{2}{3}}||u_{d,q}||_2 \tag{16}$$

$$U_{DC} = \frac{3}{\pi}(\sqrt{2}U_{RMS} - I_{DC}\omega L_s) \tag{17}$$

$$P = \frac{U_{DC}I_{DC}}{\eta} \tag{18}$$

$$Q = \sqrt{\left(\frac{P}{PF}\right)^2 - P^2} \tag{19}$$

$$i_d = \frac{1}{||u_{d,q}||_2^2}(u_d P + u_q Q) \tag{20}$$

$$i_q = \frac{1}{||u_{d,q}||_2^2}(u_q P - u_d Q) \tag{21}$$

where $||u_{d,q}||_2^2 = u_d^2 + u_q^2$ is the square of $\mathcal{L}_2$-norm. The analogous equations for the rectifier connected to the generator in the current-output mode can be formulated. The input variables for such rectifier are i_d, i_q, and U_{DC} whereas the output variables are u_d, u_q, and I_{DC}.

2) Bidirectional DC-DC Converter: A bidirectional DC-DC converter [37] (see Fig. 3 (a)) is developed using switched power junctions [38] as shown in Fig. 3 (b). Switching signals for buck and boost switches along with the operating mode are input to the model. **1s** represents the ideal switches $S1$, $S2$, $D1$ and $D2$ whereas **0s** represents the junction between the buck and boost switches.

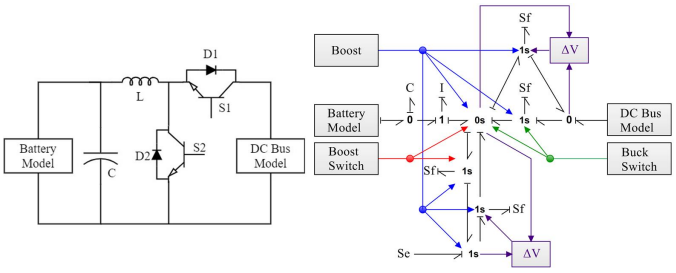

(a) (b)

Fig. 3: Bidirectional DC-DC converter models, (a) electric circuit model (b) bond graph model.

3) Voltage Source Inverter (VSI): The average model of a PWM VSI using the d-q transformation is implemented using a modified transformer (MTF) in bond graph methodology based on [12] as,

$$\begin{bmatrix} u_q \\ u_d \end{bmatrix} = m \begin{bmatrix} sin(\phi_0 - \theta) \\ cos(\phi_0 - \theta) \end{bmatrix} U_{DC} \tag{22}$$

$$I_{DC} = m(i_q sin(\phi_0 - \theta) + i_d cos(\phi_0 - \theta)) \tag{23}$$

where m is the modulation index, ϕ_0 is an initial arbitrary phase angle and θ is the d-q transformation angle.

E. Circuit Breakers

The circuit breakers are used to interface the energy carriers and loads to the bus. Moreover, buses are interconnected through the bus-tie breaker. Based on their connections and number of interfaces, two different models of circuit breakers are developed using the switched-power junctions **0s** connected with a very high resistance element [20]. A breaker with a single input-output is developed for connecting the battery or motor load through the converter to the bus (see Fig. 4 (a), whereas the generator breaker and bus-tie breaker need dual input-output interfaces (see Fig. 4 (b)).

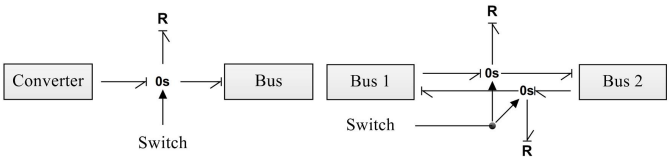

(a) (b)

Fig. 4: Circuit breaker models, (a) for battery or motor connection (b) for generator or bus-tie connection.

F. DC bus

A simplified shipboard DC bus is modeled as a connection point for the energy carriers and the loads using the switched-power junction **0s**.

III. Control System Design

A hierarchical control structure is considered efficient for the systems with several control objectives [11], [39]. The considered hybrid power system comprises several control objectives, such as bus voltage, battery current, engine speed, generator voltage, battery power, generator power, etc. Thus, three different control levels are designed for the generation side, namely tertiary, secondary, and primary control levels. The load side inverter drive is controlling the induction motor speed and torque. The controllable components, controllers, and their input and output variables are shown in Fig. 5, which gives a complete overview of the designed control architecture for a DC marine hybrid power system simulation. It also shows the major signal flows between the physical components and the control systems.

A. Tertiary Control System

EMS acts as a tertiary level control system. In this work, the EMS model decides the causality of the generator depending on the priority selection of the generator and the status of the bus-tie breaker. Moreover, rule-based EMS strategies are formulated assuming that the maximum battery discharging power (P_{BDmax}) is always less than generator optimal power (P_{Gopt}) (see Table I) based on [40]. The load power, generator power reference, minimum generator power, maximum battery charging power, and battery power reference are denoted by P_L, P_G, P_{Gmin}, P_{BCmax}, and P_B, respectively. P_L, P_G, P_{Gopt}, P_{Gmin}, and P_{BDmax} have a positive sign whereas P_{BCmax} has a negative sign. Consequently, the sign of P_B signifies whether the battery is charging (negative) or discharging (positive).

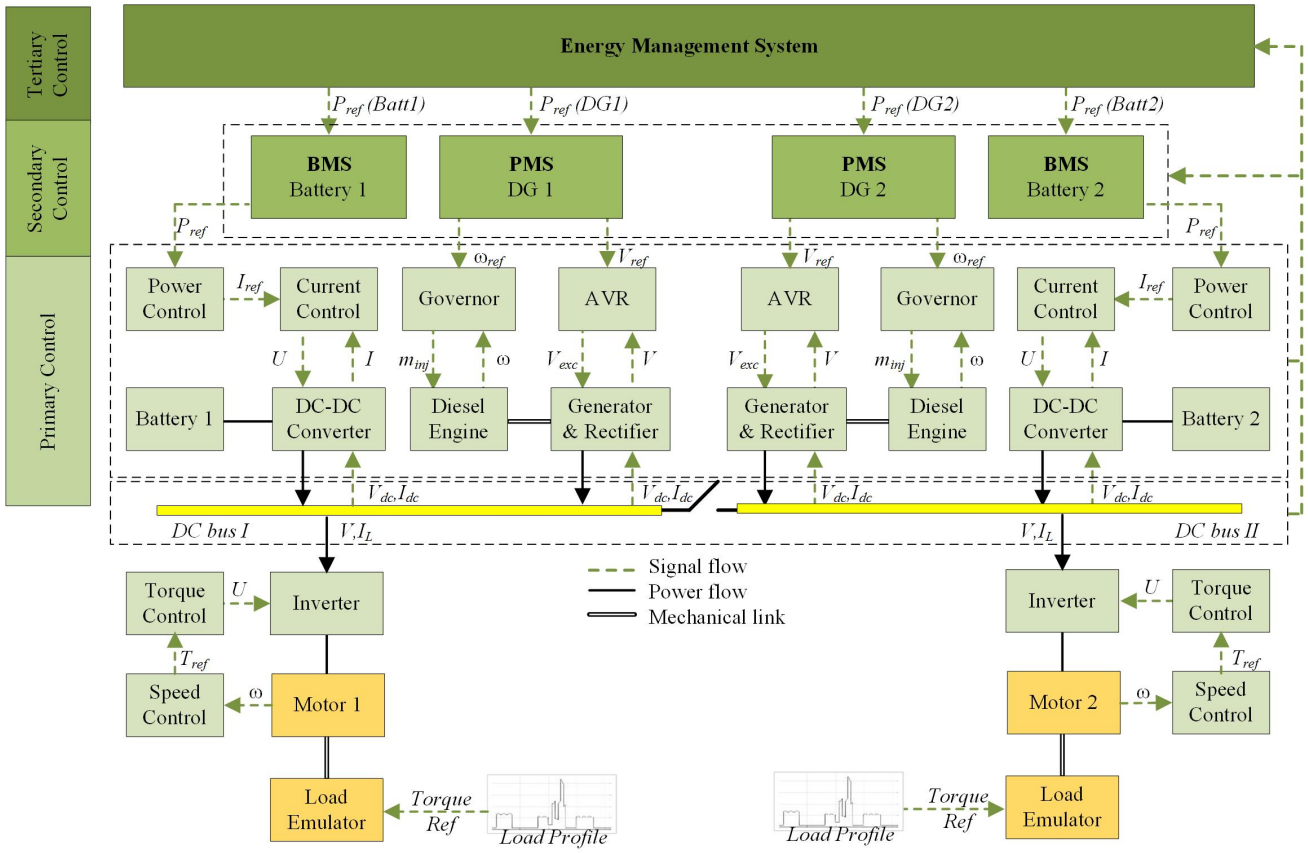

Fig. 5: Complete overview of the control system designed for a DC hybrid power system.

TABLE I: RULE-BASED EMS STRATEGIES.

	$SoC \leq SoC_{min}$	$SoC_{min} < SoC < SoC_{max}$	$SoC \geq SoC_{max}$
$P_L \leq P_{BDmax}$	$P_G=P_{Gopt}$ $P_B=P_L-P_G$ if $P_B<P_{BCmax}$ $P_B=P_{BCmax}$ $P_G=P_L-P_B$	$P_G=P_{Gmin}$ $P_B=P_L-P_G$ if $P_B>P_{BDmax}$ $P_B=P_{BDmax}$ $P_G=P_L-P_B$	$P_G=P_{Gmin}$ $P_B=P_L-P_G$ if $P_B>P_{BDmax}$ $P_B=P_{BDmax}$ $P_G=P_L-P_B$
$P_{BDmax}<P_L$ $P_L \leq P_{Gopt}$	$P_G=P_{Gopt}$ $P_B=P_L-P_G$ if $P_B<P_{BCmax}$ $P_B=P_{BCmax}$ $P_G=P_L-P_B$	$P_G=P_{Gopt}$ $P_B=P_L-P_G$ if $P_B<P_{BCmax}$ $P_B=P_{BCmax}$ $P_G=P_L-P_B$	$P_G=P_L$ $P_B=0$
$P_L>P_{Gopt}$	$P_G=P_L$ $P_B=0$	$P_G=P_{Gopt}$ $P_B=P_L-P_G$ if $P_B>P_{BDmax}$ $P_B=P_{BDmax}$ $P_G=P_L-P_B$	$P_G=P_{Gopt}$ $P_B=P_L-P_G$ if $P_B>P_{BDmax}$ $P_B=P_{BDmax}$ $P_G=P_L-P_B$

B. Secondary Control System

As the DC hybrid power system has very high dynamics, the control system should also be fast-acting. However, high load transients may easily make the system unstable. Thus to reduce the stiffness of the system, proportional controllers are used to adjusting the power references from the EMS. The voltage, speed and power references for a generator set are generated by the power management system (PMS) as,

$$V_{ref\_Gi} = V_{nom}(1 - K_{VGi}L_i) \tag{24}$$

$$\omega_{ref\_Gi} = \omega_{bi}(1 + L_i(0.5 - K_{\omega_{Gi}})) \tag{25}$$

$$P_{ref\_Gi} = P_{Gi} + (V_{nom} - V_{dc})/K_{PGi} \tag{26}$$

where, V_{ref_Gi}, ω_{ref_Gi} and P_{ref_Gi} are the reference voltage, speed and power for the i^{th} generator, respectively. $L_i = T_{Gi}\omega_{Gi}/P_{nom\_Gi}$ is the engine load fraction, K_{VGi}, $K_{\omega_{Gi}}$ and K_{PGi} are the respective control coefficients for the voltage, speed and power of i^{th} generator and ω_{bi} is the base speed for the i^{th} generator.

Similarly, for controlling the battery power flow, a simplified battery management system (BMS) generates the battery power reference for the DC-DC converter control system (CCS) as,

$$P_{ref\_Bi} = P_{Bi} - (V_{nom} - V_{dc})/K_{PBi} \tag{27}$$

where, P_{ref_Bi} and K_{PBi} are reference power signal and control coefficient respectively for the i^{th} battery. Battery dynamics is highly dependent on the state of charge (SoC) of the battery. SoC is calculated using Ah-balance as in (28), where SoC_0 is the initial SoC, C is the nominal battery capacity in Ah, I_{batt} is the battery current.

$$SoC = SoC_0 - \frac{1}{3600 \cdot C}\int_{t_0}^{t} I_{batt}dt \tag{28}$$

C. Primary Control System

The low-level control in marine power system regulates the power, voltage, current, or speed based on the reference signal obtained from the secondary controller.

1) Governor: The engine is operated with variable speed to maintain the optimal loading condition, thereby saving fuel and reducing emissions. The calculated speed reference by the PMS is then regulated using a PI controller, which provides the amount of fuel injection as,

$$m_{inj} = K_p(\omega_{ref} - \omega_m) + \frac{K_p}{T_i}\int(\omega_{ref} - \omega_m)dt \quad (29)$$

where, m_{inj} is the amount of fuel to be injected, K_p is the proportional gain, T_i is the integral time constant, ω_{ref} is the reference speed, and ω_m is the measured speed.

2) Automatic Voltage Regulator (AVR): The generator voltage is usually maintained using AVR. In this work, DC bus voltage and the generator power output are directly regulated using PI controllers, modeled as an AVR, which regulates the generator's excitation field voltage. Besides, the excitation field voltage is saturated, as mentioned in the generator specification.

$$e_v = V_{ref} - V_{dc} \quad (30)$$

$$e_p = P_{ref\_G} - P_{Gen} \quad (31)$$

$$u_{ex} = K_{pv}e_v + \frac{K_{pv}}{T_{iv}}\int e_v dt + K_{pp}e_p + \frac{K_{pp}}{T_{ip}}\int e_p dt \quad (32)$$

where u_{ex} is the field excitation voltage, K_{pv}, K_{pp} are proportional gain, and T_{iv}, T_{ip} are integral time constant. When the bus-tie breaker is closed, and both the generators are operating, the voltage references for both the generators are calculated by the voltage-control mode generator system.

3) DC-DC Converter Control: A DC-DC converter controller is modeled as a cascaded power and current controller (see Fig. 6). The battery power is calculated using the measured battery voltage and current signals. The PI controller is used to control the power output from the battery. The output from the power controller is scaled by a gain K, providing a current reference signal to the inner current controller. The current controller output is pulse-width modulated using a triangular carrier wave of 2 kHz frequency and generates the buck or boost switching signals.

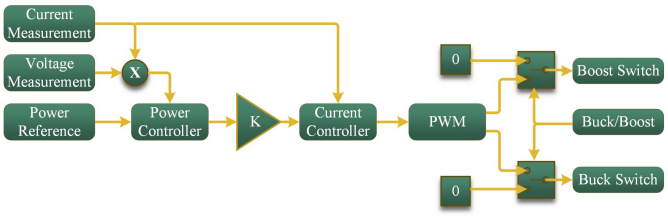

Fig. 6: Designed DC-DC converter control system.

4) Inverter Control: AC motor load is connected to the DC bus via a controllable inverter. The motor torque and speed need to be controlled in the shipboard power system. In this work, the cascaded speed-torque control is implemented as an inverter drive. The output of the speed controller gives a reference to the torque controller. The torque controller output is used as a modulation index (m) in the inverter model (see (22) - (23)). The inverter control system (ICS) can be summarized mathematically as,

$$e_\omega = \omega_r - \omega_m \quad (33)$$

$$T_r = K_p e_\omega + \frac{K_p}{T_i}\int e_\omega dt \quad (34)$$

$$e_T = T_r - T_m \quad (35)$$

$$m = K_p e_T + \frac{K_p}{T_i}\int e_T dt \quad (36)$$

where, K_p and T_i are proportional gain and integral time of a PI controller. ω_r and ω_m are reference and measured speed in rad/s for the induction motor. T_r and T_m are reference and measured torque in Nm for the induction motor.

IV. Simulation Results and Analysis

The complete system model is developed by integrating the modular component and control system models (see Fig. 7). The electrical or mechanical connections between the components are represented by the half-arrowed lines (power bonds), whereas the full-arrowed lines show the control or measurement signals. The double line indicates the vector connection whereas the single line shows the variable level connection. In the EMS, the selection of the master generator can be made using the master input, whereas loading and operating modes can be selected using the mode input. When the bus-tie breaker is closed, the master generator regulates the bus voltage, which would be the input variable for the other generator. However, both the generator maintain their respective bus voltage when the bus-tie breaker is in the open state. The propeller is not modeled, but the torque exerted by the propeller to the induction motor is an input, which can be an external load profile or the predefined loading in the load model itself.

The Runge-Kutta 4th order solver is used to solve the equations with the step size of 30 μs and data logging in a time interval of 1 ms. The system model can be run in real-time or even faster than real-time. In this case, the simulation of 40 s is solved in the computational time of 33 s. The physical component and control system parameters are summarized in Table II and Table III, respectively.

TABLE II: Rated values of component parameters.

Component	Specifications
Generator 1	4 poles, 400 kVA, 450 V, 513 A, 1.2-1.8 krpm, 2500 Nm, 10 kgm^2
Generator 2	4 poles, 230 kVA, 450 V, 295 A, 1.2-1.8 krpm, 1500 Nm, 5.9 kgm^2
Motor 1 / 2	4 poles, 160 kW, 440 V, 223 A, 1500 rpm, 1015 Nm, 2.66 kgm^2
Battery 1 / 2	Li-ion, 65 Ah, 346 V
DC Bus	565 V

The hybrid power system model can be tested using various scenarios that can occur in the real system. As there are several cases that can be simulated, few essential cases, such as ramp

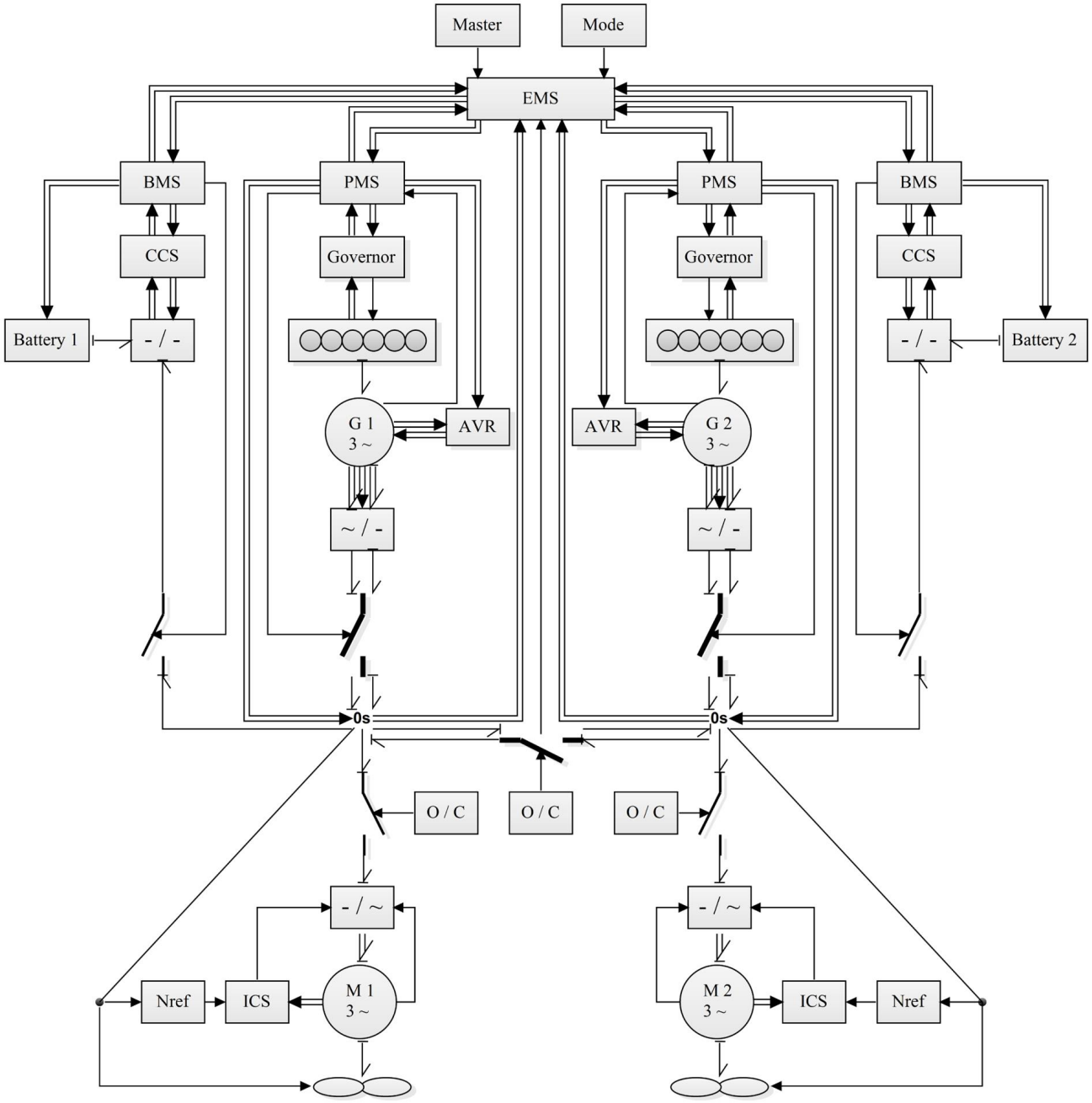

Fig. 7: A Top-level view of complete system model. CCS - Converter control system, AVR - Automatic voltage controller, O/C - Open or close command, ICS - Inverter control system, Nref - Electric motor speed reference, G - Generator, and M - Motor.

load change, speed change, step load change, bus-tie breaker operation, and component failure, are simulated for testing the proposed model. For the simulations, the system is initialized in no-load operating mode. The generators have maintained their respective bus voltages. The batteries are connected to the bus. The load breakers are closed, and the electric motors are running at 1500 rpm and with no load torque.

A. Case 1 - Ramp Load Change

The load power change on the heavy consumers, such as propulsion loads, is usually limited with the ramp rate to maintain the stability of the ship power system and ensure the safe operation of the power supply. In this case, this type of load control is investigated. A ramp function is used to change the load torque and speed references in the electric motors representing the propulsion motors.

At 10 s, the load torque in each electric motor is increased from 0 to 1000 Nm at a time interval of 1 s to simulate a ramp load. The bus-tie breaker is left open as a first scenario, and the results are depicted in Fig. 8 - 10. Each of the generator maintain their respective bus voltage by regulating their field voltage through AVR. The bus voltage reference is generated

TABLE III: CONTROL SYSTEM PARAMETERS.

PMS	BMS/CCS	AVR/Governor	ICS
K_{VGi}=0.05	K_{PBi}=0.05	K_{pv}=10	$K_{p\omega}$=50
$K_{\omega Gi}$=0.0001	K_{pp}=1.511	T_{iv}=0.1	$T_{i\omega}$=0.5
K_{PGi}=0.05	T_{ip}=0.05	K_{pp}=0.001	T_{r_min}=-1515
	P_{min}=-34600	T_{ip}=5	T_{r_max}=1515
	P_{max}=69200	K_p=0.0001	K_{pT}=0.01
	K_{pi}=3.555	T_i=0.75	T_{iT}=2.0
	T_{ii}=0.05	m_{inj_min}=0.0	m_{min}=0.0
	I_{min}=0.1	m_{inj_max}=0.26	m_{max}=1.2728
	I_{max}=0.9		

for each bus, depending on the loading percentage of the generator connected. Therefore, bus 2 has a lower voltage than the bus 1 as the loading percentage for generator 2 is higher than that of generator 1. The total load on each bus is shared by the energy carriers connected on that bus. The batteries are discharging to supply power to the bus since their voltage and SoC are high above the lower limit. At 30 s, the reference speed for motor 1 is set to 1200 rpm, and motor 2 is set to 1300 rpm while keeping the load torque constant. It resulted in lower power demand. The bus voltage (V_{Bus}), power response ($Power$), and generator AC voltage (V_{Gen}) and current (I_{Gen}) are depicted in Fig. 8. V_{Bus1} and V_{Bus2} are the bus voltage in bus 1 and bus 2, respectively. The total load power (P_L) is the sum of power exerted by motor 1 (P_{M1}) and motor 2 (P_{M2}), expressed as $P_L = P_{M1} + P_{M2}$. Similarly, the total battery power (P_B) is given as $P_B = P_{B1} + P_{B2}$, where P_{B1} and P_{B2} are battery 1 and battery 2 power, respectively. P_{G1} and P_{G2} are the active power output of generator 1 and generator 2, respectively. The phase A voltages for generator 1 and 2 are indicated as V_{G1} and V_{G2}, whereas phase A currents are indicated as I_{G1} and I_{G2}, respectively. In this case, there is no significant transient and risk of failures for the generators. However, the performance of the propulsion load is limited due to the ramp function.

With the decrease in the load power demand, there occurs less battery discharging or current flow. It resulted in less voltage drop in the internal resistance of the battery, thus increasing the terminal battery voltage level. The battery discharging rate is also reflected in battery SoC curves. The battery voltage (V_{Batt}), state of charge (SoC), and current (I_{Batt}) responses are included in Fig. 9. As generator 2 is smaller in rated capacity, battery 2 is supplying higher current than battery 1.

The speed response for the engines and motors are shown in Fig. 10, which shows that the voltage source inverters for each motor are correctly controlled to attain the required motor speed. One of the benefits of DC bus comes with the absence of bus frequency. It enhances the flexibility in the engine speed control to optimize the loading in the engine-generator, such that fuel consumption and emission are minimized. The engine speed references are regulated between 1200 rpm to 1800 rpm depending on the loading conditions. As the loading percentage for the generator 2 is higher than that of generator 1, the generator 2 is running at a higher speed than generator 1. N_{E1}, N_{E2}, N_{M1}, and N_{M2} are the speed of engine 1, engine 2, motor 1, and motor 2, respectively.

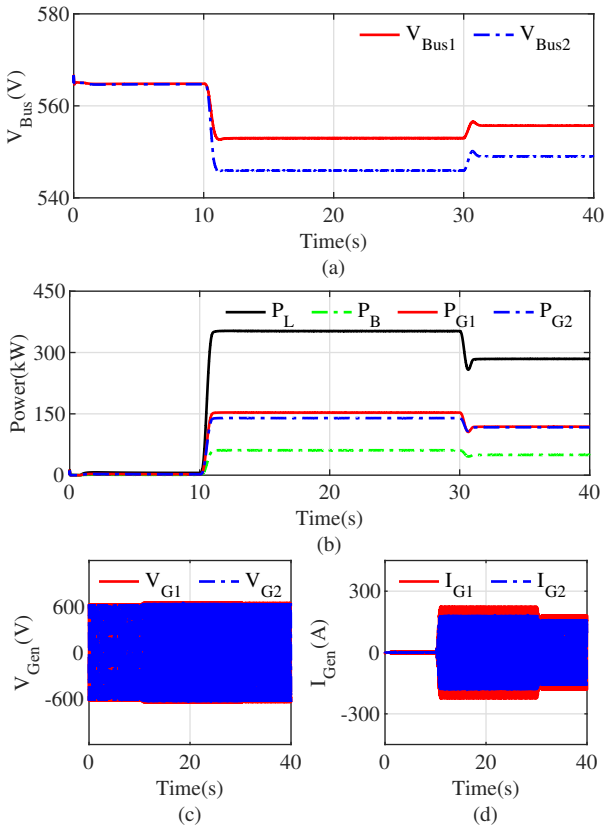

Fig. 8: Simulation results for a ramp load change followed by decreased speed setpoint to both the electric motors with bus-tie breaker in open state, (a) bus voltage, (b) power responses, (c) generator AC voltage, and (d) generator AC current.

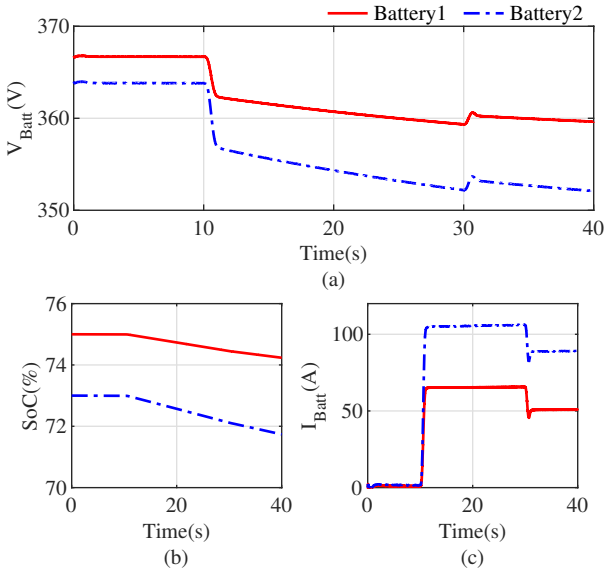

Fig. 9: Battery responses for a ramp load change followed by decreased speed setpoint to both the electric motors with bus-tie breaker in open state, (a) voltage, (b) SoC, and (c) current.

As a second scenario, the bus-tie breaker is kept closed, and generator 1 is selected as the master generator. The loading

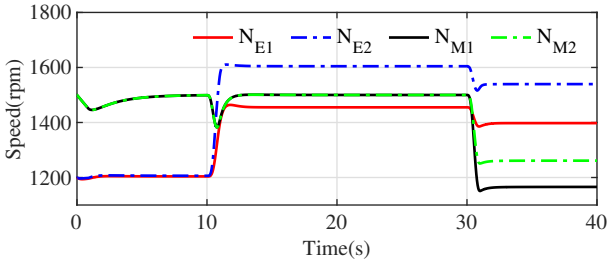

Fig. 10: Speed responses for a ramp load change followed by decreased speed setpoint to both the electric motors with bus-tie breaker in open state.

and load-sharing strategies are identical to the first scenario. However, generator power is different because the load is now shared between all four energy carriers, which means energy carriers in bus 1 also share some portion of the load in bus 2. The bus voltage and power responses for this scenario are included in Fig. 11.

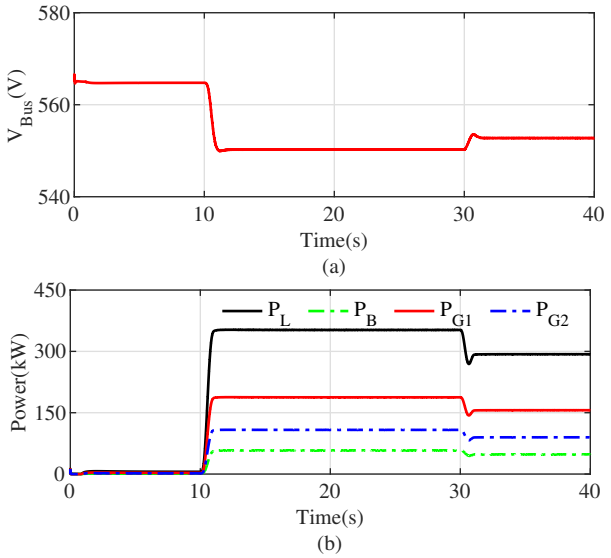

Fig. 11: Simulation results for a ramp load change followed by decreased speed setpoint to both the electric motors with bus-tie breaker in closed state, (a) bus voltage and (b) power responses.

B. Case 2 - Step Load Change

During the emergency conditions, the shipboard load can change abruptly. The power system needs to be robust enough to handle such a condition. The load torque in each motor is increased or decreased using a step function. In this case, the bus-tie breaker is closed, resulting in a shared bus. At 5 s, the total load of approximately 180 kW is applied by both electric motors. It is followed by an increase to the level of 350 kW and decrease to 90 kW and 0 kW approximately at 15 s, 25 s, and 35 s, respectively (see Fig. 12).

The power responses for the generators and batteries are smooth and stable. The undershoot and overshoot in the bus voltage are observed during the high load power transients; however, they stabilize soon and the variation is within the required limit [41]. The current waveform shows that generator 1 has a higher amplitude than generator 2, which is also reflected in power supplied by the generators. The slight voltage difference is due to the lack of voltage synchronization. One of the advantages of the DC power system is the ability to operate without synchronization. However, AVR regulates the amplitude of the DC bus voltage. The minor difference in the amplitude of V_{G1} and V_{G2} is due to the impedance of the cables and filters. Moreover, no or very less distortion in the AC waveform for the generators shows that they are robust for these high load transients.

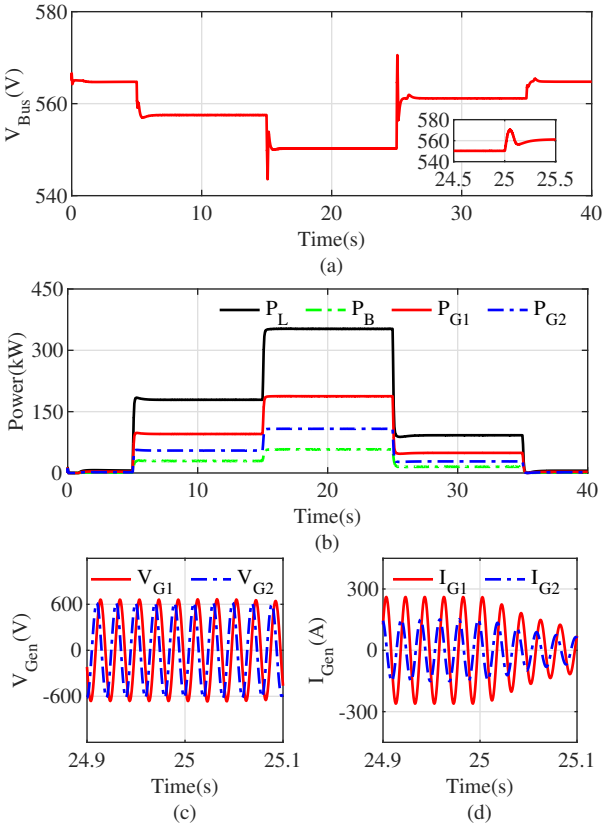

Fig. 12: Simulation results for a multiple step load change, (a) bus voltage, (b) power responses, (c) generator AC voltage, and (d) generator AC current.

C. Case 3 - Bus-tie Breaker Operation

In a shipboard power system, it is necessary to maintain redundancy to avoid a single failure event. Therefore, the power system is usually divided into two or more sections. It helps to isolate the section in case of the occurrence of failure. However, when the system is functioning properly, combining the sections may reduce the number of running generators, or a spinning reserve may serve for both sides of the bus. These conditions present the necessity of bus-tie breaker and its operation in closed or open states. In this simulation case, the ability of the modeled system in simulating bus-tie operation is presented. Initially, the bus-tie breaker is kept open. At 5 s, the 1000 Nm of load torque is applied to each electric motors

connected to two sides of the bus. At 15 s, the bus-tie breaker is closed, and at 25 s the breaker is again opened. The bus voltage, power, and generator behavior are depicted in Fig. 13. The bus voltage is maintained by respective generators when sectionalized and by the master generator (generator 1) for the shared bus.

The abrupt opening or closing of the bus-tie breaker is resulting in high bus voltage transients. These transients can be reduced by the implementation of DC voltage synchronization, consequently RMS voltage of the generators. No significant distortions in the AC waveform are observed. With the opening of the bus-tie breaker, the current amplitude through generator 2 increases while that for generator 1 decreases. The change in the power setpoint of generators is due to the load-sharing strategy.

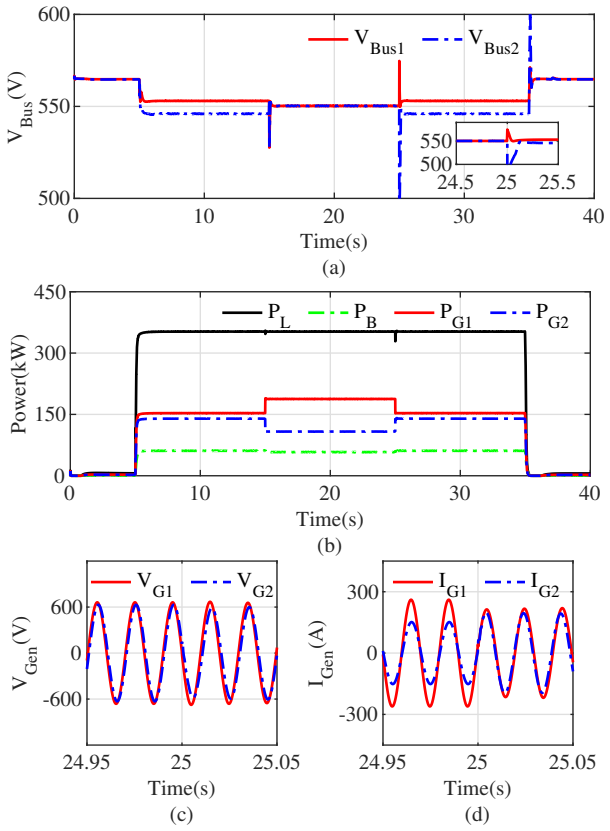

Fig. 13: Simulation results for bus-tie breaker operation, (a) bus voltage, (b) power responses, (c) generator AC voltage, and (d) generator AC current.

D. Case 4 - Component Failure

The power system model also needs to reflect the 'what-if' scenarios when any of the components or the subsystem fails. A simple simulation case is developed to show the ability of the model to simulate such a scenario. The bus-tie breaker is in a closed state, and the loading is applied at 5 s. The generator 2 breaker is abruptly opened at 20 s reflecting the real case scenarios like generator breaker trip or engine-generator trip due to any critical failures such as high cooling water temperature, low lube oil pressure, or overloading that may result in a single failure event. The bus voltage, power, and generator responses for the simulation of fault are shown in Fig. 14.

It is observed that the power system is able to run even after missing a generator; however, the bus voltage got a downward spike due to the sudden loss of current supplied by the generator 2. The current waveform for generator 1 shows high distortions compared to the voltage waveform during the sudden loss of generator 2 power. In this case, the generator 1 is forced to compensate for the loss of generator 2.

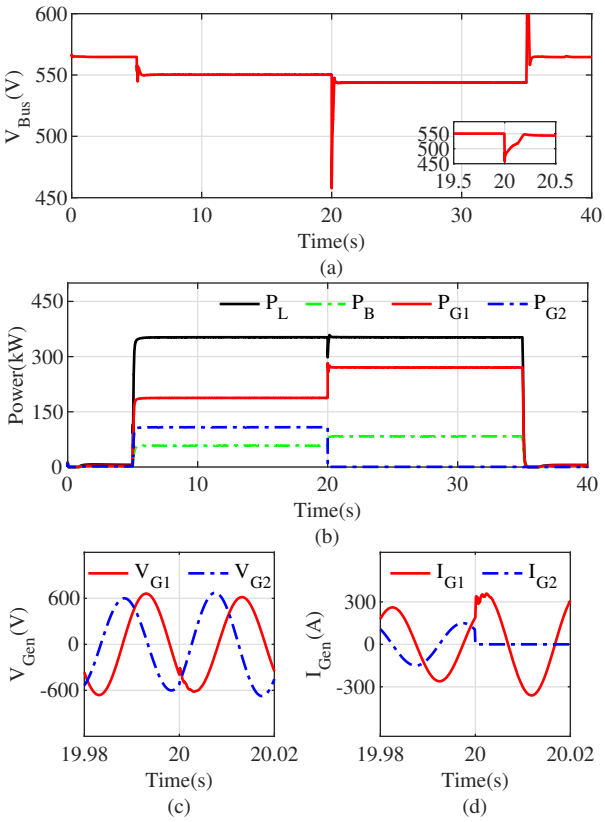

Fig. 14: Simulation results during a failure insertion, (a) bus voltage, (b) power responses, (c) generator AC voltage, and (d) generator AC current.

V. Laboratory Testing

A. System Model Validation

The full-scale lab experimental data and the harbor tugboat load profile obtained from [1], [40] is used to validate the simulation results in the system level.

The harbor tugboat operation modes can be broadly categorized into standby (idle), transit (loitering), and ship assist. The load profile implemented in the full-scale lab experiment and simulation experiment is presented in Fig. 15. The lab experiment was divided into three segments. The first segment consists of standby and transit modes. The second segment includes a transit (follow ship), standby, and ship assist modes. The third segment comprises of the standby and transit (return to the quay) modes. The three segments of the load profile (segment 1 - 660 s, segment 2 - 660 s, and segment 3 -

600 s) are simulated separately to make the simulation results comparable with the experimental results.

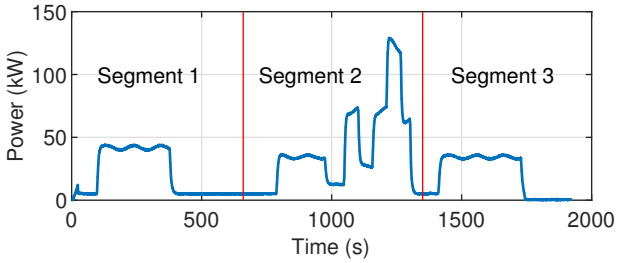

Fig. 15: Harbour tugboat load profile.

The overview of the experimental laboratory set up along with the data acquisition and control stations is depicted in Fig. 16. The measurements from the laboratory experiment are obtained from the logging system in control computers. A 65 Ah battery bank and a 400 kVA generator are used as the energy carriers, whereas an electric motor drive and brake with a nominal capacity of 160 kW are used as a load in the experimental system.

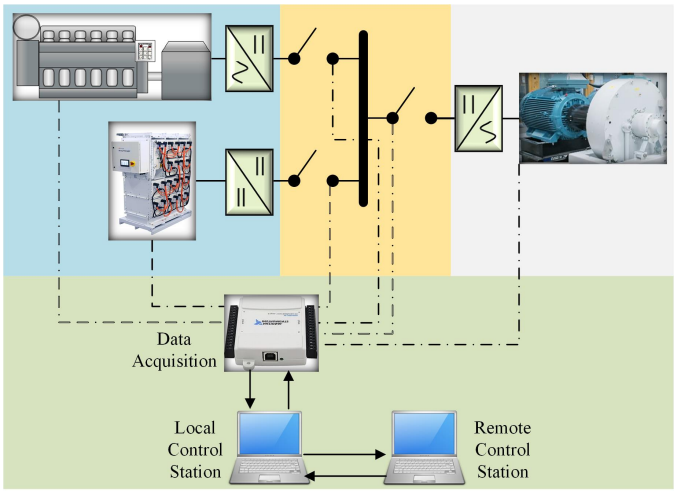

Fig. 16: Overview of the experimental setup, data acquisition and control stations.

The time-series load profile is converted and fed into the induction motor as a load torque. The simulation system parameters are as presented in Section IV. The bus-tie breaker is kept open, and the power system with generator set 1, battery 1, and motor 1 is operated. The set up is initialized to operating mode with battery and load circuit breakers in a closed state, engine running at 1200 rpm, and induction motor at 1500 rpm. After some experiments with the ship load profile and comparison with experimental results, K_{VGi} is tuned to 0.124.

The simulation and experimental results for all three segments are presented in Fig. 17. The bus voltage (V_{bus}), generator power (P_{gen}), battery power (P_{batt}), and battery state of charge (SoC) responses obtained from the simulation is compared with the experimental results for the same load power profile (P_{load}). P_{batt} is positive when the battery is discharging and it is negative when the battery is charging. It is observed that the dynamics obtained from the simulation are matching well with the experimental results in all three segments. A spike in the bus voltage is observed during the transition from one mode to another, for instance, from the standby to the transit mode. Moreover, the variable speed operation of the engine allows it to produce optimal power. Depending on load demand, the generator and battery supply power in such a way that the engine can operate in its higher efficiency region while the battery compensates for the under or overload conditions by discharging or charging, respectively. In segment 2 and 3, some discrepancies between the experimental and simulation results are observed when the battery SoC is higher than 82.5%.

The incorrect voltage measurement or failures in the battery charger may lead to the local overcharging [42]. The overcharging of a battery may result in thermal instability, structural damage, and gas evolution [43]. It is, therefore, essential to avoid overcharging. The experimental results show that the battery charging power is reduced when the battery is charged over 82.5% to ensure the safety limits. Since commercial control modules are used in the laboratory, the exact control algorithm is not known. In this work, the overcharging of the battery is handled by reducing the charging power in steps based on the SoC of the battery (see Table IV). The charging power reductions are derived manually by the inspection of the experimental results. Some deviations in the bus voltage and generator power output are also observed due to the battery charging power deviations.

TABLE IV: BATTERY CHARGING POWER REDUCTION FOR HIGHER SOC.

SoC(%)	Charging power (%)	C-rate
SoC $\geq$ 82.5	89.50	1.38
SoC $\geq$ 83.0	66.50	1.02
SoC $\geq$ 84.0	43.35	0.67
SoC $\geq$ 84.5	23.12	0.36

The deviation between the experimental and simulated results are further evaluated to quantify the performance of the system model using root mean square error (RMSE) and presented in Table V. The average RMSE between the experimental and simulated results for all the measured system variables are well within 10 eu. It shows that the system model's accuracy is good enough for its further use in system design, analysis, and testing.

TABLE V: THE EXPERIMENTAL AND SIMULATED OUTPUT DEVIATIONS EXPRESSED IN RMSE.

Output	Segment 1	Segment 2	Segment 3	Avgerage
V_{bus} (V)	1.4636	3.8395	2.1237	2.4756
P_{gen} (kW)	4.1512	7.0627	6.9632	6.0590
P_{batt} (kW)	2.3157	5.3784	5.3923	4.3621
SoC (%)	0.4860	0.3471	0.5317	0.4549

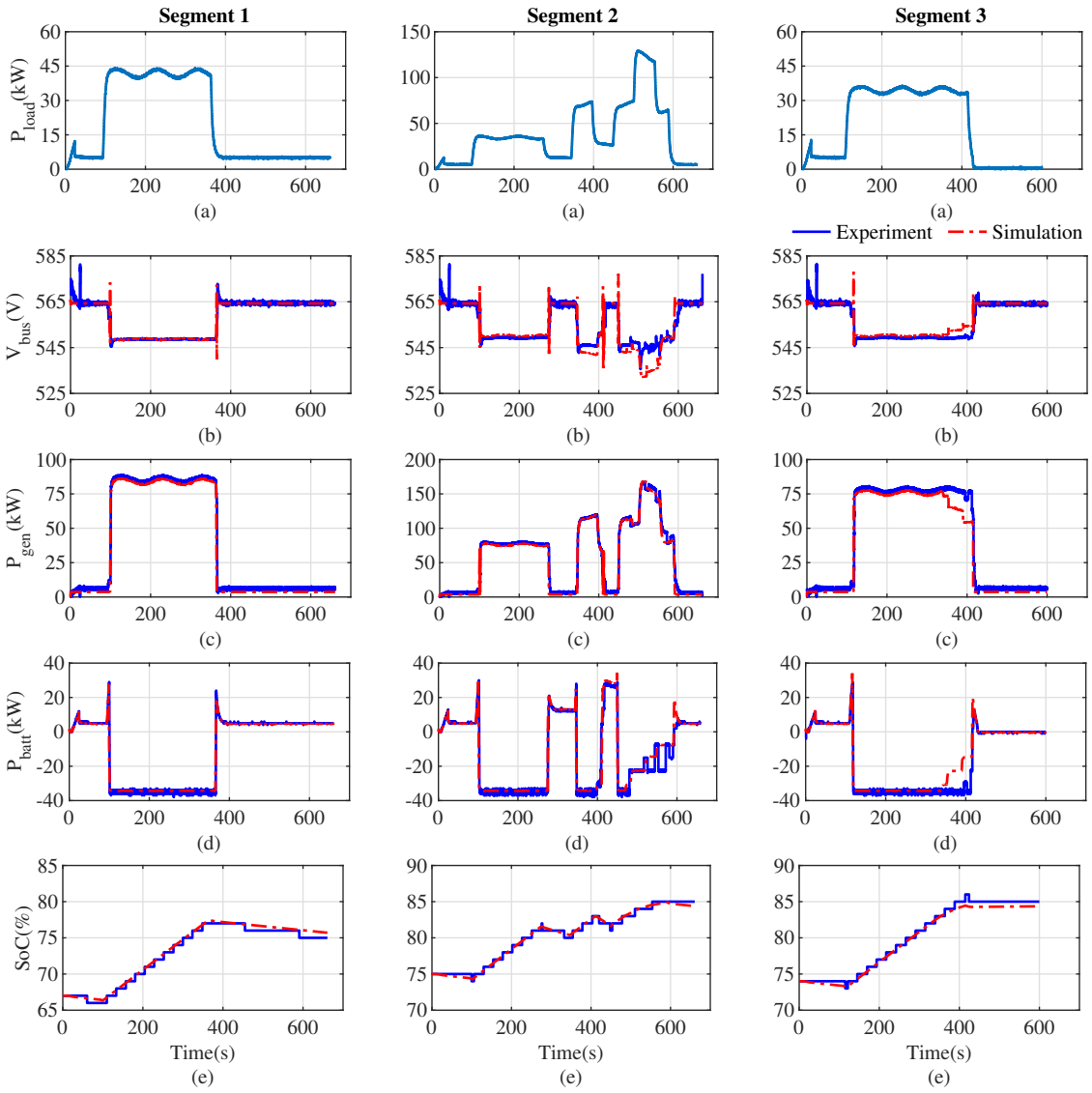

Fig. 17: System model validation with the experimental results for all three segments, (a) load profile (b) bus voltage (c) generator power (d) battery power (e) battery SoC.

B. Bus Voltage Deviation

The class societies have limited the allowable voltage tolerance to $\pm 10\%$ [41] for the DC bus voltage. The bus voltage RMSE from nominal value for the experiment was 13.28 V, whereas 14.92 V for the simulation results in segment 2 (see Fig. 17 - V_{bus}). The instantaneous bus voltage drop for less than 50% loading of the generator is quite high. Hence, the bus voltage deviation analysis is performed using a time-scaled down version of the load profile presented in Fig. 15. Decreasing the control coefficient for generator voltage in PMS from 12.4% to 5 % decreased the voltage deviation from the nominal voltage considerably while keeping other responses similar. However, decreasing the control coefficient too much may lead the system voltage to oscillate for high load transients.

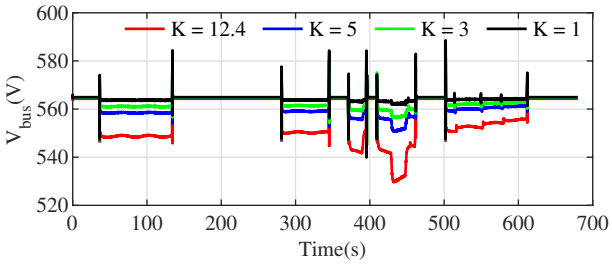

Fig. 18: Bus voltage comparison for different control coefficients.

VI. Conclusion

In this work, a bond graph-based DC hybrid power system model has been developed by integrating component models with varying degrees of fidelity. The system model is reconfigurable to develop various DC hybrid power system

architectures due to the modularity in the component models. The ability of the modeled system to capture necessary dynamics during various scenarios, such as load change, propulsion speed change, bus-tie breaker operation, and failure condition, is presented. Further, the modeled system is tested with the experimental results for a ship load profile. The system-level testing has shown that the system model is accurate enough to estimate the necessary dynamics of the real system. Moreover, the developed system model is used to analyze the bus voltage deviation in the experimental setup. It suggests that decreasing the control coefficients in the experimental setup improves the RMS deviation of bus voltage; however, decreasing it too much may increase the maximum error. The developed system model acts as a platform for the simulation of marine DC hybrid power systems for various 'what-if' scenarios. It will also serve as a baseline for sophisticated system modeling and analysis, such as efficiency analysis, power system design, and failure studies.

The computational efficiency presented by the system is fairly good as it can simulate faster than real-time. Most of the computational burden is created by switching frequency of power electronics converters, which requires the whole system model to be solved in a minimal time interval and with high computational effort. However, modularity helps to exchange different fidelity of component models according to the test requirements. Further, using the co-simulation framework, the component models with faster dynamics can be solved with higher frequency while other components with relatively lower frequency. It can decrease the computational effort while maintaining accuracy.

ACKNOWLEDGMENT

The authors would like to thank Muzaidi B. Othman and Tegoeh Tjahjowidodo for providing the laboratory data.

REFERENCES

[1] M. B. Othman, N. P. Reddy, P. Ghimire, M. K. Zadeh, A. Anvari-Moghaddam, and J. M. Guerrero, "A Hybrid Power System Laboratory: Testing Electric and Hybrid Propulsion," *IEEE Electrification Magazine*, vol. 7, DOI 10.1109/MELE.2019.2943982, no. 4, pp. 89–97, Dec. 2019.

[2] M. U. Mutarraf, Y. Terriche, K. A. K. Niazi, J. C. Vasquez, and J. M. Guerrero, "Energy storage systems for shipboard microgrids—A review," Dec. 2018.

[3] E. Çabukoglu, G. Georges, L. Küng, G. Pareschi, and K. Boulouchos, "Battery electric propulsion: an option for heavy-duty vehicles? Results from a Swiss case-study," *Transportation Research Part C: Emerging Technologies*, vol. 88, DOI 10.1016/j.trc.2018.01.013, pp. 107–123, Mar. 2018.

[4] ABS, "ABS Advisory on Hybrid Electric Power Systems," American Bureau of Shipping, Tech. Rep., 2017.

[5] J. O. Lindtjørn, F. Wendt, B. Gundersen, J. F. Hansen, A. As, M. Coe, and O. Vessels, "Demonstrating the Benefits of Advanced Power Systems and Energy Storage for DP Vessels," *Dynamic Positioning Conference*, pp. 1–24, 2014.

[6] J. Ling-Chin and A. P. Roskilly, "Investigating the implications of a new-build hybrid power system for Roll-on/Roll-off cargo ships from a sustainability perspective – A life cycle assessment case study," *Applied Energy*, vol. 181, DOI 10.1016/J.APENERGY.2016.08.065, pp. 416–434, Nov. 2016.

[7] R. D. Geertsma, R. R. Negenborn, K. Visser, and J. J. Hopman, "Design and control of hybrid power and propulsion systems for smart ships: A review of developments," *Applied Energy*, vol. 194, DOI 10.1016/j.apenergy.2017.02.060, pp. 30–54, May. 2017.

[8] A. J. Sorensen, R. Skjetne, T. Bo, M. R. Miyazaki, T. A. Johansen, I. B. Utne, and E. Pedersen, "Toward Safer, Smarter, and Greener Ships: Using Hybrid Marine Power Plants," *IEEE Electrification Magazine*, vol. 5, DOI 10.1109/mele.2017.2718861, no. 3, pp. 68–73, Sep. 2017.

[9] M. R. Miyazaki, A. J. Sorensen, N. Lefebvre, K. K. Yum, and E. Pedersen, "Hybrid modeling of strategic loading of a marine hybrid power plant with experimental validation," *IEEE Access*, vol. 4, DOI 10.1109/ACCESS.2016.2629000, pp. 8793–8804, 2016.

[10] S. S. Kevin Koosup Yum , Stian Skjong, Bhushan Taskar, Eilif Pedersen, "Simulation of a Hybrid Marine Propulsion System in Waves," in *28th CIMAC World Congress*, no. June, 2016.

[11] R. Nilsen and I. Sorfonn, "Hybrid Power Generation Systems," in *13th European Conference on Power Electronics and Applications*, pp. 1–9, Barcelona, Spain, 2009.

[12] B. Zahedi and L. E. Norum, "Modeling and Simulation of All-Electric Ships With Low-Voltage DC Hybrid Power System," *IEEE Transactions on Power Electronics*, vol. 28, DOI 10.1109/TPEL.2012.2231884, no. 10, pp. 4525–4537, Oct. 2013.

[13] M. K. Zadeh, R. Gavagsaz-Ghoachani, J. P. Martin, S. Pierfederici, B. Nahid-Mobarakeh, and M. Molinas, "Discrete-Time Tool for Stability Analysis of DC Power Electronics-Based Cascaded Systems," *IEEE Transactions on Power Electronics*, vol. 32, DOI 10.1109/TPEL.2016.2526740, no. 1, pp. 652–667, Jan. 2017.

[14] E. Skjong, T. A. Johansen, M. Molinas, and A. J. Sorensen, "Approaches to Economic Energy Management in Diesel-Electric Marine Vessels," *IEEE Transactions on Transportation Electrification*, vol. 3, DOI 10.1109/TTE.2017.2648178, no. 1, pp. 22–35, Mar. 2017.

[15] M. K. Zadeh, L. M. Saublet, R. Gavagsaz-Ghoachani, B. Nahid-Mobarakeh, S. Pierfederici, and M. Molinas, "Energy management and stabilization of a hybrid DC microgrid for transportation applications," in *Conference Proceedings - IEEE Applied Power Electronics Conference and Exposition - APEC*, vol. 2016-May, DOI 10.1109/APEC.2016.7468355, pp. 3397–3402. Institute of Electrical and Electronics Engineers Inc., May. 2016.

[16] N. P. Reddy, D. Pasdeloup, M. K. Zadeh, and R. Skjetne, "An Intelligent Power and Energy Management System for Fuel Cell/Battery Hybrid Electric Vehicle Using Reinforcement Learning," in *ITEC 2019 - 2019 IEEE Transportation Electrification Conference and Expo*, DOI 10.1109/ITEC.2019.8790451. Institute of Electrical and Electronics Engineers Inc., Jun. 2019.

[17] T. A. Pedersen and E. Pedersen, "Bond graph modelling of marine power systems," *Mathematical and Computer Modelling of Dynamical Systems*, vol. 18, DOI 10.1080/13873954.2011.603735, no. 2, pp. 153–173, 2012.

[18] T. I. Bø, A. R. Dahl, T. A. Johansen, E. Mathiesen, M. R. Miyazaki, E. Pedersen, R. Skjetne, A. J. Sørensen, L. Thorat, and K. K. Yum, "Marine Vessel and Power Plant System Simulator," *IEEE Access*, vol. 3, DOI 10.1109/ACCESS.2015.2496122, pp. 2065–2079, 2015.

[19] F. Perabo and M. K. Zadeh, "Modelling of a Shipboard Electric Power System for Hardware-in-the-Loop Testing," DOI 10.1109/itec48692.2020.9161719, pp. 69–74. Institute of Electrical and Electronics Engineers (IEEE), Aug. 2020.

[20] S. Skjong and E. Pedersen, "A real-time simulator framework for marine power plants with weak power grids," *Mechatronics*, vol. 47, DOI 10.1016/J.MECHATRONICS.2017.09.001, pp. 24–36, Nov. 2017.

[21] D. Park and M. K. Zadeh, "Dynamic Modeling and Stability Analysis of Onboard DC Power System for Hybrid Electric Ships," in *ITEC 2019 - 2019 IEEE Transportation Electrification Conference and Expo*, DOI 10.1109/ITEC.2019.8790505. Institute of Electrical and Electronics Engineers Inc., Jun. 2019.

[22] M. K. Zadeh, R. Gavagsaz-Ghoachani, B. Nahid-Mobarakeh, S. Pierfederici, and M. Molinas, "Stability analysis of hybrid AC/DC power systems for more electric aircraft," in *Conference Proceedings - IEEE Applied Power Electronics Conference and Exposition - APEC*, vol. 2016-May, DOI 10.1109/APEC.2016.7467910, pp. 446–452. Institute of Electrical and Electronics Engineers Inc., May. 2016.

[23] M. K. Zadeh, R. Gavagsaz-Ghoachani, S. Pierfederici, B. Nahid-Mobarakeh, and M. Molinas, "Stability Analysis and Dynamic Performance Evaluation of a Power Electronics-Based DC Distribution System with Active Stabilizer," *IEEE Journal of Emerging and Selected Topics in Power Electronics*, vol. 4, DOI 10.1109/JESTPE.2015.2484218, no. 1, pp. 93–102, Mar. 2016.

[24] F. M. Uriarte and R. Hebner, "Development of a multicore power system simulator for ship systems," in *2011 IEEE Electric Ship Technologies Symposium, ESTS 2011*, DOI 10.1109/ESTS.2011.5770850, pp. 106–110, 2011.

[25] F. M. Uriarte, R. E. Hebner, and A. L. Gattozzi, "Accelerating the Simulation of Shipboard Power Systems," in *Grand Challenges in Modeling & Simulations (GCMS2011)*, The Hague, Netherland, 2011.

[26] P. Ghimire, N. P. Reddy, M. K. Zadeh, E. Pedersen, and J. Thorstensen, "Dynamic Modeling and Real-Time Simulation of a Ship Hybrid Power System Using a Mixed-Modeling Approach," DOI 10.1109/itec48692.2020.9161520, pp. 1–6. Institute of Electrical and Electronics Engineers (IEEE), Aug. 2020.

[27] S. Skjong and E. Pedersen, "On the numerical stability in dynamical distributed simulations," *Mathematics and Computers in Simulation*, vol. 163, DOI 10.1016/j.matcom.2019.02.018, pp. 183–203, Sep. 2019.

[28] D. Karnopp, D. L. Margolis, and R. C. Rosenberg, *System dynamics : modeling, simulation, and control of mechatronic systems*. Wiley, 2012.

[29] P. C. Breedveld, "Port-based modeling of mechatronic systems," *Mathematics and Computers in Simulation*, vol. 66, DOI 10.1016/j.matcom.2003.11.002, no. 2-3, pp. 99–128, Jun. 2004.

[30] P. J. Gawthrop and G. P. Bevan, "Bond-graph modeling - A tutorial introduction for control engineers," *IEEE Control Systems*, vol. 27, DOI 10.1109/MCS.2007.338279, no. 2, pp. 24–45, Apr. 2007.

[31] T. N. Madhusudan, "A review of Bond-graph representation based design methodologies," Tech. Rep., 1995.

[32] J. D. Herbst, A. L. Gattozzi, A. Ouroua, and F. M. Uriarte, "Flexible test bed for MVDC and HFAC electric ship power system architectures for Navy ships," in *2011 IEEE Electric Ship Technologies Symposium, ESTS 2011*, DOI 10.1109/ESTS.2011.5770843, pp. 66–71, 2011.

[33] D. Sahm, "A two-axis, bond graph model of the dynamics of synchronous electrical machines," *Journal of the Franklin Institute*, vol. 308, DOI 10.1016/0016-0032(79)90113-3, no. 3, pp. 205–218, 1979.

[34] K. Benabdelaziz and M. Maaroufi, "Battery dynamic energy model for use in electric vehicle simulation," *International Journal of Hydrogen Energy*, vol. 42, DOI 10.1016/J.IJHYDENE.2017.05.165, no. 30, pp. 19 496–19 503, Jul. 2017.

[35] L. I. Silva, J. Jaguemont, C. H. De Angelo, and L. Boulon, "Modeling an Electric Vehicle Lithium-Ion Battery Pack Considering Low Temperature Behavior," in *2016 IEEE Vehicle Power and Propulsion Conference (VPPC)*, DOI 10.1109/VPPC.2016.7791727, pp. 1–5. IEEE, Oct. 2016.

[36] Y.-S. Lee and M. H. Chow, "Diode Rectifiers," *Power Electronics Handbook*, DOI 10.1016/B978-0-12-811407-0.00007-6, pp. 177–208, Jan. 2018.

[37] M. S. Saleh, A. Althaibani, Y. Esa, Y. Mhandi, and A. A. Mohamed, "Impact of clustering microgrids on their stability and resilience during blackouts," in *2015 International Conference on Smart Grid and Clean Energy Technologies (ICSGCE)*, DOI 10.1109/ICSGCE.2015.7454295, pp. 195–200. IEEE, Oct. 2015.

[38] A. C. Umarikar and L. Umanand, "Modelling of switching systems in bond graphs using the concept of switched power junctions," *Journal of the Franklin Institute*, vol. 342, DOI 10.1016/j.jfranklin.2004.08.005, no. 2, pp. 131–147, 2005.

[39] J. M. Guerrero, J. C. Vasquez, J. Matas, L. G. de Vicuna, and M. Castilla, "Hierarchical Control of Droop-Controlled AC and DC Microgrids—A General Approach Toward Standardization," *IEEE Transactions on Industrial Electronics*, vol. 58, DOI 10.1109/TIE.2010.2066534, no. 1, pp. 158–172, Jan. 2011.

[40] L. W. Chua, T. Tjahjowidodo, G. G. Seet, and R. Chan, "Implementation of optimization-based power management for all-electric hybrid vessels," *IEEE Access*, vol. 6, DOI 10.1109/ACCESS.2018.2883324, pp. 74 339–74 354, 2018.

[41] P. Ghimire, D. Park, M. K. M. Zadeh, J. Thorstensen, and E. Pedersen, "Shipboard Electric Power Conversion: System Architecture, Applications, Control, and Challenges [Technology Leaders]," *IEEE Electrification Magazine*, vol. 7, DOI 10.1109/MELE.2019.2943948, no. 4, pp. 6–20, Dec. 2019.

[42] Z. J. Zhang, P. Ramadass, and W. Fang, "Safety of Lithium-Ion Batteries," in *Lithium-Ion Batteries: Advances and Applications*, pp. 409–435. Elsevier B.V., Jan. 2014.

[43] A. S. Mussa, M. Klett, M. Behm, G. Lindbergh, and R. W. Lindström, "Fast-charging to a partial state of charge in lithium-ion batteries: A comparative ageing study," *Journal of Energy Storage*, vol. 13, DOI 10.1016/j.est.2017.07.004, pp. 325–333, Oct. 2017.

Pramod Ghimire received the M.Sc. degree in Systems and Control Engineering from Telemark University College, Norway, in 2012. He has been working as a software engineer at the Department of Maritime Simulation, Kongsberg Digital, Norway, since 2012. Currently, he is an industrial Ph.D. candidate at the Department of Marine Technology, NTNU. His current research interests include mathematical modeling and simulation, marine hybrid power system, efficiency analysis of the hybrid power system, and data-driven modeling.

Mehdi Zadeh received the Ph.D. degree in Electrical Engineering from NTNU, Trondheim, Norway, in 2016. From 2016 to 2017, he was with the power electronics industry, working on the development of battery charging systems. In 2017, he joined the Marine Technology Centre at NTNU in Trondheim, where he is currently an Associate Professor of Hybrid Power Systems and the director of the Marine Electrification Research Lab. His main research interests include ship electrification for low-emission and autonomous shipping, onboard DC power systems, and offshore renewable energy systems.

Eilif Pedersen received the M.Sc. degree in Marine Engineering from the Norwegian Institute of Technology, Norway, in 1983. He has been with the Norwegian Marine Technology Research Institute, as a Senior Research Engineer until 1999, where he joined the NTNU as an Associate Professor. He has held multiple positions, such as a Vice Dean of Education with the Faculty of Engineering Science and Technology, the Head of Master Programs in marine technology, the Leader with the Research Group of Marine Systems, and the Head of Machinery Laboratory at the Department of Marine Technology. His areas of expertise are in the field of modeling methodology and simulation of dynamic multidisciplinary and mechatronic systems focusing on machinery system dynamics, internal combustion engines, vibrations, thermal- and hydraulic machines, fuel-cell system dynamics, and hybrid power plants for marine applications.

Jarle Thorstensen received the M.Sc. degree in Cybernetics and Robotics from the NTNU, in 1987. He worked as software developer at the Institute of Energy Technology, Norway, from 1987 to 1989. From 1989 to 1990, he was with Autodisplay, Norway as a section leader for vehicle LCD pilot production. Since 1990, he is with Kongsberg Group, and currently working as a senior research and development engineer at the Department of Maritime Simulation. His current research interests include modeling and simulation of various ship systems and hybridization of ship power systems.